2022 International Conference on Manipulation, Automation and Robotics at Small Scales (MARSS) | 978-1-6654-5973-0/22/$31.00 ©2022 IEEE | DOI: 10.1109/MARSS55884.2022.9870255

SerpenBot, a Laser Driven Locomotive Microrobot for Dry Environments using Learning Control

Zhong Yang, *Student Member, IEEE*, Moath Alqatamin, *Member, IEEE* Andriy Sherehiy, *Member, IEEE*, Ruoshi Zhang, *Member, IEEE*, Mojtaba Al Hudibi, *Student Member, IEEE* Nazita Taghavi, *Member, IEEE*, Dan O. Popa, *Senior Member, IEEE*

***Abstract*— In this paper, we introduce the Serpenbot, a microrobot smaller than 1mm in size that is powered via laser energy and operates in dry environments. The microrobot achieves locomotion on a Si substrate by selective coupling of laser energy between its two legs. The coupling mechanism is achieved by laser beam selective irradiation of the microrobot's body to initiate the gait. Multi-Physics Models developed in our past work are difficult to use in formulating a microrobot controller. Therefore, in this paper, the microrobot model is simplified to differential drive kinematics that approximates the robot behavior, and the model was used to formulate a neural-network learning controller that can steer the robot to desired locations on the silicon substrate. Simulations predict the robot position regulation achieved by learning of the inverse robot Jacobian. Preliminary experimental results are also presented to confirm that this steering controller will also work in practice.**

Keywords: Microrobot, Microassembly, Microfactory, Steering Control, Neural Network Learning

I. INTRODUCTION

Microrobotics has seen considerable progress in the last 30 years. Similar to macro-scale robots, microrobots can walk, swim, fly, change their position and affect their environment. The vast majority of mobile microrobots operate in wet environments, where the surface forces dominate their operation. The nonlinear nature of these surface forces make it challenging to design, simulate, and fabricate the microrobots with controllable behavior.

Due to the size limitations, most microrobots must harvest energy from the environment [1-4, 6-10]. The environment can also be utilized for the robot control, as in the case of physical fields, for instance electrical and magnetic. So far, many microrobots are powered and controlled with the help of magnetic fields which are particularly suitable for medical applications [1-4]. Electric fields were also used to control the behavior of bacteria-powered microrobots (BPM) [5]. Acoustic actuation is another method utilized in a study [6,7] focused on the robot which motion is controlled by tuning the frequency of the ultrasound energy.

In the last two decades, several research groups also considered and employed laser light as a way to power and control micorobots. The choice of laser light as an actuation method is dictated by its inherent and diverse properties, such as directionality, optical coherence, high efficiency of power density (intensity per area), control of size and shape of the irradiated area, and waveform - continuous or pulsed mode of operation. For example, RoboBee is a flying microrobot with integrated solar cells, which when irradiated with a laser, are powering piezoelectric actuators coupled with wings [8]. A similar principle was applied in the micro-swimmer also using solar cells to set the robot into motion [9]. In another study, [10], while light-tweezer effects have been used to drive micro-gripper [11]. In summary, current studies proves a good control for microrobots operating in a liquid environment by different actuation means with potential major applications in medicine and nanotechnology. However, mobile micro robotic systems in dry environments are seldomly studied since surface effects in these environments are much stronger and less predictable.

In this paper, we present our sub-mm laser driven microrobot, SerpenBot, which was fabricated from a Si wafer using a novel, two-layer Deep Reactive Ion Etching process. SerpenBot utilizes an opto-thermo-mechanical conversion effect to achieve locomotion on dry surfaces. It is driven by microscale thermal actuators which are sequentially engaged when irradiated by a pulse laser. Laser enables motion and steering control as well acting as a power supply. In our previous work [12-16], we have shown that steering control of the Chevbot and SerpenBot microrobots in dry environments can be realized in two ways, namely 1) tuning the laser frequency, and 2) off-axis irradiation of the robot's body. In this work we focused on the latter steering control method and propose a Neural – Network Learning Control scheme for motion control. The approach was implemented as a PID Neural Right-Forward-Left (PID-N-RFL) controller, is based on neural network learning and was verified through simulation. Preliminary experimental results verify our steering strategy, confirming that SerpenBot can travel along selected trajectories for significant distances in the cm range, with translational velocities in the range of 1 ~ 100 μm/s.

This paper is organized as follows: Section II includes details about SerpenBot design and fabrication; Section III describes steering strategy and its modeling. Section IV introduces a control scheme based on neural network solutions validated in simulation; Section V includes details on laser experimental setup, results and discussion; Finally, Section VI is a summary of main findings.

II. SERPENBOT DESIGN AND FABRICATION

SerpenBot is a laser-driven microrobot with approximate dimension $450\mu m \times 540\mu m \times 40\mu m$, that shares

* This work was supported by NSF Grants 1734383, 1849213. Authors are with the Louisville Automation and Robotics Research Institute, University of Louisville, Kentucky, USA, Email: zhong.yang@louisville.edu.

978-1-6654-5973-0/22/$31.00 ©2022 IEEE

locomotion principles with its predecessor, the ChevBot [12,13]. The SerpenBot has two asymmetrical thermal actuators, called Elbow Thermal Actuator (ETA), implemented as legs shown in Fig. 1 and 2. Actuation by stick and slip principle is achieved by laser irradiation on the microrobot body, at selective locations, power levels, and pulse frequencies. When the laser radiates on the surface of the microrobot, cyclic thermal expansion drives the motion on the robot legs. A stick and slip forward motion observed through a microscope is generated due to 20 µm thick dimples attached to the 20 µm thick robot body. By varying the center of the laser beam selectively onto each leg, turning behavior can be achieved regardless of oscillation resonant frequency which determines forward and turning velocity. A recent study [16], identified both theoretical and experimental methods to evaluate different SerpenBot designs, and led to selection of best fitting candidates for further investigation with regards to steering control. The chosen design parameters for the SerpenBots studied in our paper is shown in Fig. 1.

In our past work with ChevBots and SerpenBots, their fabrication process included an assembly step to connect the robot body and dimple with the help of the UV adhesive. Unfortunately, this introduced significant difficulties in maintaining robot dimensional precision and required delicate steps of aligning the dimple with the microrobot's body using a dedicated microassembly station [13]. Moreover, during operation, we often experienced decomposition of the UV adhesive at elevated temperatures during laser irradiation.

We recently developed a new assembly-less fabrication process in which SerpenBot's dimple is manufactured directly on the body of the microrobot in the cleanroom, thus eliminating the need for additional assembly steps and the use of UV adhesive (Fig. 2). The new fabrication process uses a Silicon on Insulator (SOI) wafer with 40um thickness device layer, and selectively etches away the device layer through 10 process steps depicted in Fig. 3 and summarized below:

1) 300nm SiO_2 growth by Plasma-enhanced chemical vapor deposition (PECVD), as a protection layer for the dimple.
2) First photolithography with Shipley 1813 photoresist.
3) Removal of SiO_2 by buffered oxide etch (BOE) solution.
4) Removal of the photoresist by N-Methyl-2-pyrrolidone (NMP) bath.
5) Second photolithography with Shipley 1813 photoresist.
6) A first deep reactive ion etching (DRIE) process, to create the body of the microrobot.
7) Etch photoresist by oxygen plasma in the DRIE tool.
8) A second DRIE step to create the dimple of the microrobots. The thickness of the body and the dimple is 20µm and 40µm, respectively, measured from the buried oxide (BOX) layer.
9) Removal of the photoresist through an NMP bath.
10) Release the microrobot from wafer substrate by vapor hydrogen fluoride (VHF) etching.

After completing the successful fabrication of SerpenBot, its microrobot tethers are broken, the robot is removed from the release die, and placed on a transfer die. Finally, it is transferred on a 2-inch Si wafer substrate (arena) for laser steering experiments.

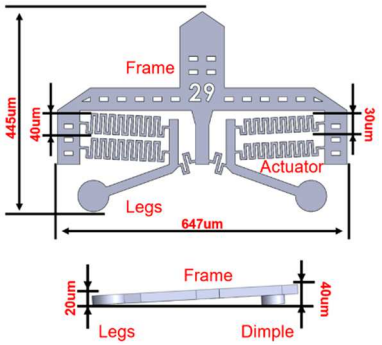

Fig. 1 Designs of serpentbots used in this study showing top and side views.

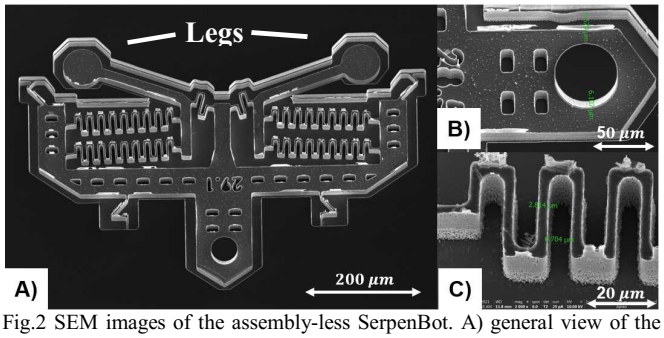

Fig.2 SEM images of the assembly-less SerpenBot. A) general view of the tethered microrobot, B) fabricated circular dimple, C) serpentine structures of the robot's actuator.

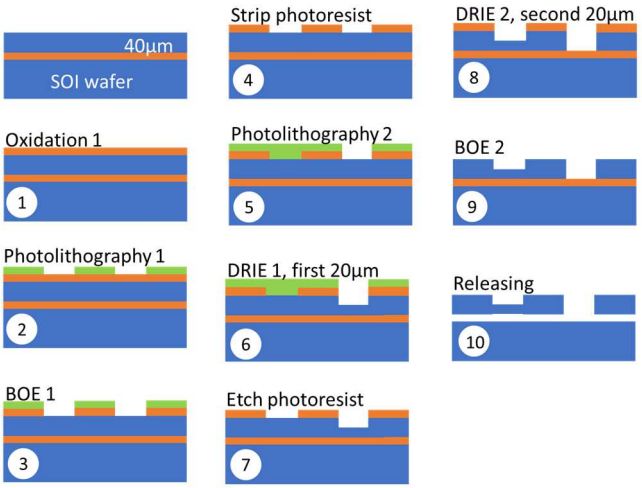

Fig. 3 Cleanroom fabrication process steps for the assembly-less SerpenBot.

III. System Modeling

A. Kinematic Models

Our previous study on laser-driven microrobots [14] revealed that their motion is governed by complex Multiphysics opto-thermal-mechanical phenomena. Models of these phenomena are also dependent on thermal boundary conditions and intermittent contact with the substrate. Practically, it is difficult to use such models to design a robot controller, since they are complex and computationally costly to implement using Finite Element Analysis.

The physics-based dynamic modeling of ChevBot shows that these microrobots can be described as complex nonlinear third order systems with many unknown or hard to measure parameters. Nevertheless, we can use linear kinematic model to simulate the approximated behavior of the robot. Since the

original system is third order, referring to [15], we have showed that the dominant pole of the SerpenBot system is from mechanical vibration. To approximate the behavior of the legs of the robot, we can use a second order system function which represents the frequency response of the actuators.

The kinematics of the robot is the mapping between leg velocity in local frame and robot velocity in global frame depicted in Fig. 4A, and represented by states $\dot{q}^R = \begin{bmatrix} \dot{x}^R \\ \dot{y}^R \end{bmatrix}$, $\dot{q}^G = \begin{bmatrix} \dot{x}^G \\ \dot{y}^G \\ \dot{\theta}^G \end{bmatrix}$, in which $\dot{x}^R$ and $\dot{y}^R$ are the velocity of the robot legs in the local frame, while $\dot{x}^G$, $\dot{y}^G$, $\dot{\theta}^G$ are the linear and angular velocities of the robot in the global frame. The relationship between $\dot{q}^R$ and $\dot{q}^G$ can be described through the Jacobian matrix of the robot J_{rob} as:

$$\dot{q}^R = J_{rob}\dot{q}^G. \tag{1}$$

Through numerical difference expansion and integration, we can approximate the robot location in a discrete-time fashion according to:

$$\begin{bmatrix} x_k^G \\ y_k^G \\ \theta_k^G \end{bmatrix} = \begin{bmatrix} \cos\theta_{k-1}^G & -\sin\theta_{k-1}^G & 0 \\ \sin\theta_{k-1}^G & \cos\theta_{k-1}^G & 0 \\ 0 & 0 & 1 \end{bmatrix} \begin{bmatrix} \frac{1}{2} & \frac{1}{2} \\ 0 & 0 \\ -\frac{1}{l} & \frac{1}{l} \end{bmatrix} \begin{bmatrix} \dot{x}_l^R \\ \dot{x}_r^R \end{bmatrix} \Delta t + \begin{bmatrix} x_{k-1}^G \\ y_{k-1}^G \\ \theta_{k-1}^G \end{bmatrix} \tag{2}$$

where k represents a time step index, l is distance between the legs of the robot, and Δt is the sampling time. Since the motion of the leg occurs only along one direction parallel to X_R, we can use scalars $\dot{x}_l^R$and $\dot{x}_r^R$ to represent the robot right leg and left leg velocity. These velocities can be described as a function of pulsed laser energy and frequency inputs as:

$$\dot{x}_{l,r}^R = \frac{K_l I}{\sqrt{\left[1-\left(\frac{f}{f_n}\right)^2\right]^2 + \left[2\zeta\left(\frac{f}{f_n}\right)\right]^2}} \tag{3}$$

where f_n is the actuator resonant frequency, ζ is damping ratio, K_l is the gain of the laser, an empirical value, and I is the laser current.

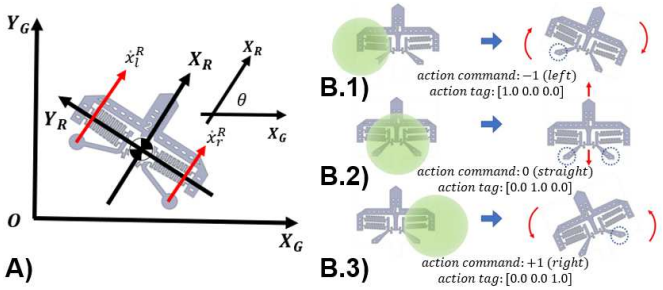

Fig. 4 Serpentbot steering scheme based on selective irradiation. A) kinematic model of the SerpenBot B.1) clockwise (counter-clockwise) motion, B.2) forward (backward) motion, B.3) counterclockwise (clockwise) motion. (Red arrows represent orientation and direction of the motion. Dashed circles indicate which actuator pair and leg is activated. Green circle represents laser spot irradiating selected part of microrobot.

B. *Control strategy*

By describing the motion of the SerpenBot as a differential drive robot, if we can realize a scenario where each leg of the robot moves at different pace (different velocity), we can change the turning behavior of the robot. Therefore, our control strategy involves laser beam heating of selected actuator of the robot each time we want to drive different leg, and in a result to run the whole SerpenBot in a desired direction. We called this scheme depicted in Fig. 4B Right-Forward-Left control (RFL).

IV. SERPENBOT CONTROLLER DESIGN

To develop a controller for the SerpenBot and implement the steering strategy, we must consider a scheme in which the laser spot position is synchronized with respect to the motion of the microrobot on the substrate. In our microrobot driving system, the substrate is moved under a fixed laser spot delivered from a 532nm green pulsed laser unit. Our control system consists of two main parts: 1) visual servoing for laser sport control and 2) steering robot behavior control. Since the SerpenBot is moving on the arena and the position of laser spot is fixed, the visual servoing system is continuously keeping the robot under the laser beam (Fig.4B). Furthermore, the microscope camera provides feedback to always keep the robot in the center of the field of view. The robot steering behavior control system consists of PID Neural Right-Forward-Left (PID-N-RFL) scheme that irradiates selected microrobot's actuators (left actuator, right actuator or both), while the varying intensity of the laser beam (laser diode current) can be used to change the turning radius of the robot. To describe our controller, we refer to Fig. 4A showing what the microscope image (camera's field of view (FOV)) of the robot will look like, while the overall control block diagram is shown in Fig. 5.

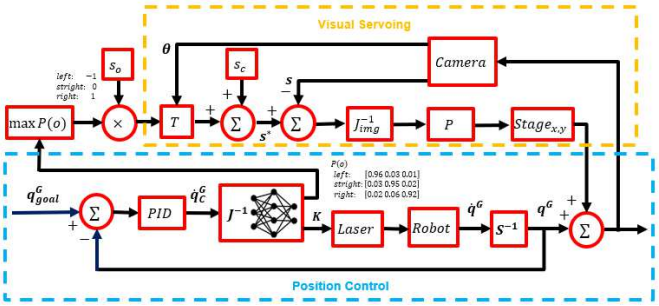

Fig. 5 Visual servoing and neural steering control block diagram.

A. *Visual Servoing*

A visual servoing controller is necessary to track robot during its motion by keeping it irradiated, e.g., within the same area in a FOV of a camera, with the help of motorized x-y stages located under the robot arena. In this arrangement, control error is the difference between robot current location in pixel coordinates s, and desired point in FOV of camera - center of the FOV (center) s_c plus the offset s_o (for left/right actuators). Error mapping serves as a control value for the x-y stages and is realized with the help of inverse image Jacobian matrix J_{img}^{-1} for transformation from pixel space to Cartesian space of x-y stages. (Fig. 5)

The image Jacobian matrix is described as follows:

$$\dot{s} = J_{img}\dot{q}^G = \begin{bmatrix} \frac{\partial s_x}{\partial x^G} & \frac{\partial s_x}{\partial y^G} & \frac{\partial s_x}{\partial \theta^G} \\ \frac{\partial s_y}{\partial x^G} & \frac{\partial s_y}{\partial y^G} & \frac{\partial s_y}{\partial \theta^G} \end{bmatrix} \begin{bmatrix} \dot{x}^G \\ \dot{y}^G \\ \dot{\theta}^G \end{bmatrix} \tag{4}$$

We can identify the image Jacobian matrix by acquiring set of random points based on the motion of the motorized x-y stages

and recording from the smart camera, as a result, the regression equation for identification of the image Jacobian is [17]:

$$J_{img,k+1} = J_{img,k} + \frac{\left(\Delta s_k - J_{img,k}\Delta q_k\right)\Delta q_{G,k}^T}{\Delta q_{G,k}^T \Delta q_{G,k}} \quad (5)$$

Where $\Delta s_k = s_k - s_{k-1}$ and $\Delta q_{G,k} = q_{G,k} - q_{G,k-1}$. After identifying Image Jacobian matrix, we implemented only proportional (P) controller, determining control equation:

$$q_{G,k+1} = q_{G,k} + K_{img}\left(J_{img}^T J_{img}\right)^{-1} J_{img}^T (s^* - s), \quad (6)$$

where K_{img} is the gain of the control value for visual servoing, and $s^* = s_c + s_o$.

B. PID Turning Controller

The PID Neural Right-Forward-Left (PID-N-RFL) controller's purpose is to realize automated motion control of SerpenBot in order to reach the commanded goal location. The PID controller shown in Fig. 5 maps the error between current configuration $(x_c^G, y_c^G, \theta_c^G)$ and goal configuration $(x_d^G, y_d^G, \theta_d^G)$ by setting the robot velocity in polar coordinate $\dot{q}_C^G = \begin{bmatrix} v_c^G \\ \omega_c^G \end{bmatrix}$, where forward velocity v_c^G and turning velocity ω_c^G as:

$$v_c^G = K_v \cdot \sqrt{e_x^2 + e_y^2}. \quad (7)$$

$$\omega_c^G = PID(e_\theta), \quad (8)$$

where K_v is the gain for linear velocity, $e_x = x_c^G - x_d^G$, $e_y = y_c^G - y_d^G$ and $e_\theta = \theta_c^G - \theta_d^G$, with θ_d^G defined as:

$$\theta_d^G = atan2(e_x, e_y). \quad (9)$$

The control variable C belongs to a semi-discrete domain, $C \in \{c|O \otimes K, O \in \{-1,0,1\}, K \in [0,1]\}$, including discrete operations RFL O, and continuous laser current gain K normalizing the laser current between 3A to 5A. Hence, we use a neural network to approximate J_{rob}^{-1} as a bridge mapping the continuous value of the PID controller to be semi-discrete space of the actual control value which is $C = J_{rob}^{-1}\dot{q}_C^G$. The neural network approximating J_{rob}^{-1}, is shown in Fig. 6.

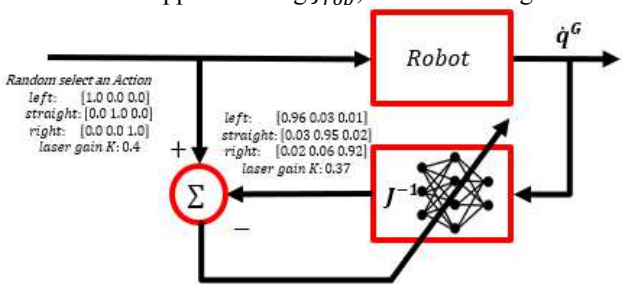

Fig. 6 Learning scheme of the inverser robot Jacobian.

We used supervised learning method to train the neural network with tags defined as right, forward, and left for representing the RFL and the laser gain values. For training the system, these tags and the normalized laser current are randomly selected as actions. After applying actions to the system, the system output is related to the microrobot state velocity $\dot{q}^G$, expressed as a pair with scalar velocity $v^G = \sqrt{(\dot{x}^G)^2 + (\dot{y}^G)^2}$ and angular velocity $\omega^G = \dot{\theta}^G$ of the robot is sent back to the neural network. At the end of training process, the neural network acts as a classifier which finds the occurrence probability of the input actions. However, during the training process, the difference of the tags and output probabilities with the laser gain will back propagate to update the parameters of the neural network. Finally, the neural network learns to get the current states of the microrobot as input and finds the laser behavior RFL as output. That makes the neural network J_{rob}^{-1} a classifier as well as a tool to calculate the inverse kinematics of the robot.

In practice, we constructed our neural network using PyTorch(® open-source library with two hidden layers of 256 neurons each and selected tanh, as activation function for the hidden layers. The output layer includes four outputs: right, forward, and left (defined tags) as well as laser gain. The activation function for RFL was softmax while the sigmoid was the activation function for the laser gain in this layer.

Fig. 7 presents training results of the proposed neural network. For this process, we first use the kinematic model to train the neural network, then through transfer leaning, we can continue training the neural network with experimental data collected based during steering. It is evident that the loss function converges to very small value under the pre-described threshold, demonstrating the promising ability of the neural network to model the robot inverse kinematic from image data.

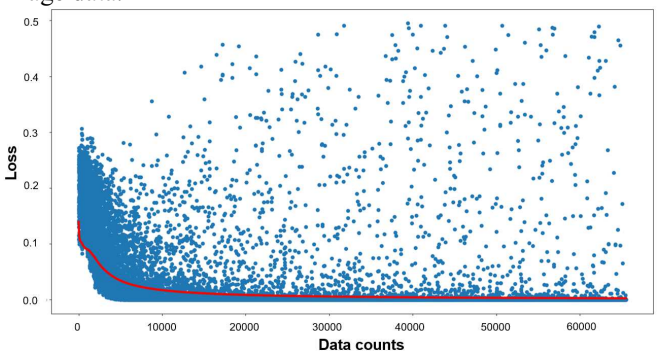

Fig. 7 The loss functions during the learning process represented by blue dots after 70000 training points. The red line is the average loss during learning.

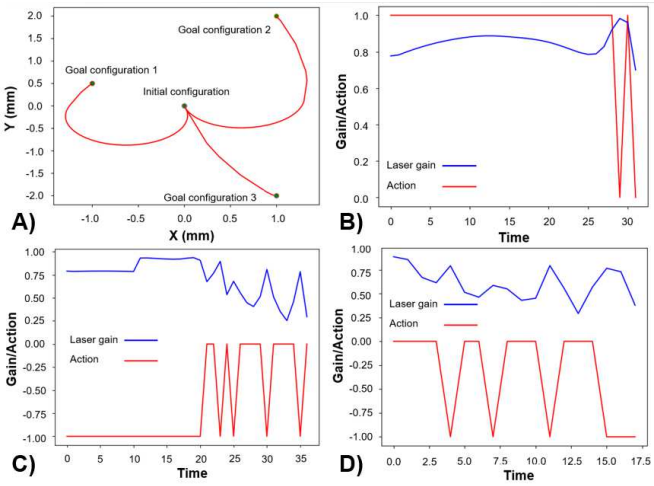

Fig. 8 A) simulation results of the controller reaching random goal locations, B, C, D) the control parameters for reaching the goal locations in A).

While training our neural network we have simulated the robot to drive and steer with three distinct states: left, forward, or right depending on the laser irradiation of the selected part

of SerpenBot (Fig. 8). Simulation results show that we were able to realize three different trajectories necessary for microrobot control: clockwise/counter clockwise revolutions, and translational motion.

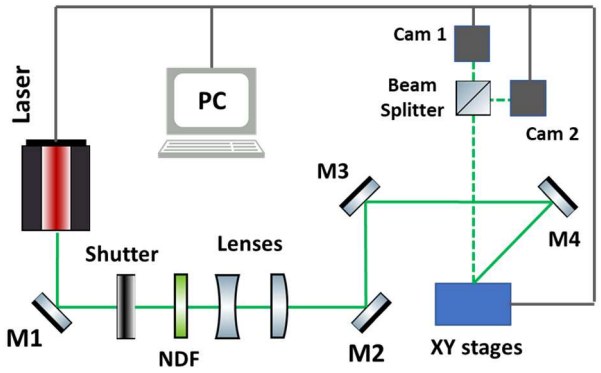

Fig. 9 Schematic of experimental setup for SerpenBot steering control.

V. Experimental Methods and Results

A schematic view of the experimental setup to drive the SerpenBot is presented in Fig. 9. As source of laser light for microrobot's actuation, we have used high power Nd:YAG pulse laser (Spectra-Physics Explorer® one) with wavelength of 532 nm. The pulse frequency can be adjusted between 0.5-60 kHz, the pulse time width and average output power can be adjusted between 10-40 ns and 0-2 W respectively. A variable neutral density filter (NDF) followed by the Uniblitz optical shutter is used to attenuate laser beam during experiments. System of two lenses adjacent to NDF allows adjustment of the size of laser spot and position of the laser beam is adjusted by varying tilt of 4 mirrors (M1-M4). Two cameras integrated with beam splitter are attached to tube lens: one, a National Instrument real-time smart camera (ISC-1780) is used for visual servoing; second, Pixelink PL-D734, is used as real time visual feedback for SerpenBot. The microrobots are placed on an arena (2-inch Si wafer) which is secured on a sample chuck, positioned on top of four cascaded linear stages. Two of stages are manually controlled for adjustments, the rest two are motorized (PI Q-521), controlled by National Instrument LabVIEW used for automated tracking and control of SerpenBot's motion. Custom LabVIEW user interface (UI) allows adjustment of the laser spot position relative to the SerpenBot's body thus allowing irradiation of the selected actuator and in result semi-automated method of steering the robot (Fig 4).

We have conducted a series of preliminary experiments to validate our proposed steering strategy involving selective actuation by irradiating specific parts of the SerpenBot. In a first stage we have tested whether selective irradiation of the left or right or both actuators would result in an expected and repeatable behavior - motion in a specific direction. In a second stage we have driven SerpenBot along the planned path of specific shapes.

A. *SerpenBot steering through selective irradiation*

We have conducted series of experiments in order to verify our steering method. Using our LabVIEW UI, we have irradiated specific part of the SerpenBot and observed behavior of our microrobot. Results show that we can realize clockwise and counterclockwise rotation depending on which actuator was under the laser beam (Fig 10).

As it can be seen recorded trajectories are elliptical in shape and for clockwise motion, we have noticed significant drift of the center of rotation (Fig. 10 E). Nevertheless, motion is repeatable and relatively stable, with respect to uninterrupted propulsion through laser irradiation, making it possible to realize number of revolutions continuously (Fig 10 C,D,E,F).

Combining these three types of SerpenBot's motion (Fig 10) allows us to direct and move microrobot in a desired location. Hence it verifies our steering strategy and enables future experimental implementation of the proposed control scheme based on the neural network, as described in Section IV. Next step is testing of our strategy by realizing different planned trajectories with the help of LabVIEW UI.

B. *SerpenBot motion along specific trajectories*

For this experiment a rectangular trajectory shape was selected as a planned path (Fig. 11). The position of the laser beam relative to serpent's body was controlled with the help of LabVIEW UI. In this experiment laser frequency was kept constant at $1700\ Hz$ with laser power was $430mW$ and we used burst mode with 50 pulses pe burst and delay time between bursts of $300ms$.

The steering mechanism following the trajectory in Fig. 11 can be described in the following way:

1) section AB and BC – microrobot is initially at rest and starts to move forward along straight line upon exposure to a laser light focused on the center of SerpentBot.
2) point **C** – robot turns left after the laser beam was focused on left actuator of the SerpentBot.
3) section **CD** – laser beam is focused back on center of SerpenBot which moves in forward direction; around ¾ of the CD section robot starts to drift sliglty to the left;
4) point **D** - robot turns left after the laser beam was focused on a left section of robot;
5) section **DE** – laser beam is focused on center againc - robot moves in forward direction;
6) point **E** – robot turns left again;
7) section **EB** and **BF** – finally, beam is focused on a center of the robot; at point **B** it intersects section **AC** and stops at **F**, after the laser beam is shut off.

Aplying similar steering strategy we were able to move and control SerpenBot along trajectories of different shapes (Fig. 11). For rectangular, triangular, and trapezoidal shapes of paths (Fig. 11 B,C,D) we followed the same trajectory as in Fig. 10, switching position of the laser beam depending on the part of the motion. However for the circualr trajectory (Fig. 10 C) we have kept laser beam focused on one of the actuators continuesly during during the whole travel.

Trajectories shown in the Fig. 11 B, C, D are less stable than "circular" one (Fig. 10 C), which is related to the fact that during motion along the straight path, robot's tends to uncontrollably turn, thus continueing adjustments has to be made during the motion by human user inputs with the help of LabVIEW UI. In future, optmimiation of the motion to acquire more smoother trajectories, can be realised through full

automation of the robot's steering by implementig our proposed PID-N-RFL control scheme.

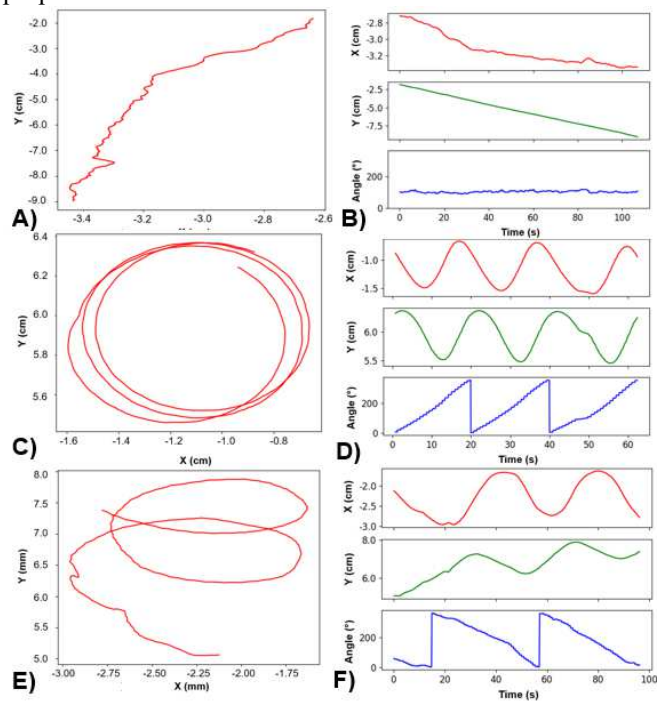

Fig. 10 Experimental results representing three basic types of SerpenBot motion – on the left trajectories; on the right recorded position (XY) and angle variation with respect to time: A,B) translational motion, C, D) counterclockwise rotation, E, D) clockwise rotation.

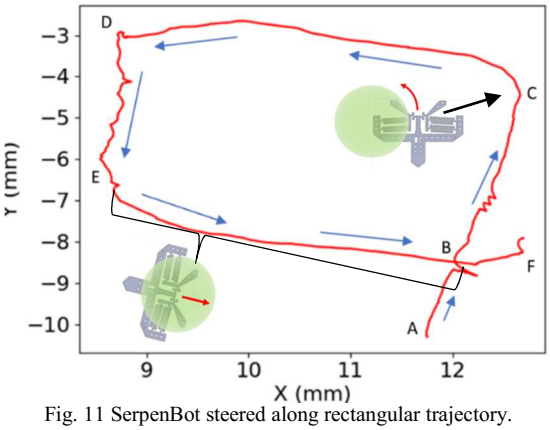

Fig. 11 SerpenBot steered along rectangular trajectory.

VII Conclusion and Future Work

In this paper we presented a novel design of assembly-less laser driven microrobot on dry surfaces, SerpenBot, along with new fabrication process, which simplified assembly procedures and optimized experimental operation involving laser irradiation. We have proposed new steering strategy for SerpenBot based on the selective irradiation of the microrobot's body, which was verified experimentally. Experimental results show that we have a sufficient steering control enabling realization of various planned trajectories at average linear speed between 10-100 µm/s. It is suggested that proposed steering mechanism is a robust approach which allows overcoming the difficulties related to complex surface effects at microscale in dry environments. Furthermore, we have conducted simulations of the steering control scheme based on the implementation of the neural network solutions. In future, we will continue development of the neural network based solutions for microrobot motion control. An integration of galvanometer in our experimental set up would allow us an optimized automated control of laser spot position on the SerpenBot's body.

References

[1] B. J. Nelson, I. K. Kaliakatsos, and J. J. Abbott, "Microrobots for Minimally Invasive Medicine," *Annual Review of Biomedical Engineering*, vol. 12, no. 1, pp. 55–85, 2010.

[2] L. Zhang, J. J. Abbott, L. Dong, B. E. Kratochvil, D. Bell, and B. J. Nelson, "Artificial bacterial flagella: Fabrication and magnetic control," *Applied Physics Letters*, vol. 94, no. 6, p. 064107, 2009.

[3] E. B. Steager, M. Selman Sakar, C. Magee, M. Kennedy, A. Cowley, and V. Kumar, "Automated biomanipulation of single cells using magnetic microrobots," *The International Journal of Robotics Research*, vol. 32, no. 3, pp. 346–359, 2013.

[4] X. Hu, I. C. Yasa, Z. Ren, S. R. Goudu, H. Ceylan, W. Hu, and M. Sitti, "Magnetic soft micromachines made of linked microactuator networks," *Science Advances*, vol. 7, no. 23, 2021.

[5] H. Kim and M. J. Kim, "Electric field control of bacteria-powered Microrobots using a static obstacle avoidance algorithm," *IEEE Transactions on Robotics*, vol. 32, no. 1, pp. 125–137, 2016.

[6] C. Dillinger, N. Nama, and D. Ahmed, "Ultrasound-activated ciliary bands for microrobotic systems inspired by Starfish," *Nature Communications*, vol. 12, no. 1, 2021.

[7] T. Luo and M. Wu, "Biologically inspired micro-robotic swimmers remotely controlled by ultrasound waves," *Lab on a Chip*, vol. 21, no. 21, pp. 4095–4103, 2021.

[8] N. T. Jafferis, E. F. Helbling, M. Karpelson, and R. J. Wood, "Untethered flight of an insect-sized flapping-wing microscale aerial vehicle," *Nature*, vol. 570, no. 7762, pp. 491–495, 2019.

[9] M. Z. Miskin, A. J. Cortese, K. Dorsey, E. P. Esposito, M. F. Reynolds, Q. Liu, M. Cao, D. A. Muller, P. L. McEuen, and I. Cohen, "Electronically integrated, mass-manufactured, Microscopic Robots," *Nature*, vol. 584, no. 7822, pp. 557–561, 2020.

[10] J. G. Glückstad, M. J. Villangca, D. Z. Palima, and A. R. Bañas, "Light-actuated microrobots for biomedical science," *SPIE Newsroom*, 2017.

[11] D. Zhang, A. Barbot, B. Lo, and G. Z. Yang, "Distributed Force control for Microrobot manipulation via planar multi-spot Optical Tweezer," *Advanced Optical Materials*, vol. 8, no. 21, p. 2000543, 2020.

[12] R. Zhang, A. Sherehiy, Z. Yang, D. Wei, C. K. Harnett, and D. O. Popa, "ChevBot – an untethered microrobot powered by laser for Microfactory applications," *2019 International Conference on Robotics and Automation (ICRA)*, 2019.

[13] R. Zhang, A. Sherehiy, D. Wei, Z. Yang, M. N. Saadatzi, and D. O. Popa, "Tracking experiments with ChevBot: A laser-actuated stick-slip Microrobot," *2019 International Conference on Manipulation, Automation and Robotics at Small Scales (MARSS)*, 2019.

[14] Z. Yang, A. Sherehiy, S. S. Chowdhury, D. Wei, R. Zhang, and D. O. Popa, "Design, fabrication and experimental validation of a steerable, laser-driven microrobot in dry environments," *2020 IEEE 16th International Conference on Automation Science and Engineering (CASE)*, 2020.

[15] Z. Yang, M. N. Saadatzi, R. Zhang, A. Sherehiy, D. Wei, C. K. Harnett, and D. O. Popal, "Multiphysics dynamic model validation methodology for laser-driven Microrobots," *2019 IEEE 15th International Conference on Automation Science and Engineering (CASE)*, 2019.

[16] S. S. Chowdhury, Z. Yang, P. W. Clapacs, and D. O. Popa, "Untethered Microrobots with serpentine actuators: The role of Elastics Point Contact & laser beam shape on their locomotion," *Volume 2: Manufacturing Processes; Manufacturing Systems; Nano/Micro/Meso Manufacturing; Quality and Reliability*, 2021.

[17] J. M. Sebastián, L. Pari, C. González, and L. Ángel, "A new method for the estimation of the image jacobian for the control of an uncalibrated joint system," *Pattern Recognition and Image Analysis*, pp. 631–638, 2005.